Uncertainty and disturbance Observer-Based Cooperative Formation Flight Control

Journal:	*Journal of Guidance, Control, and Dynamics*
Manuscript ID	2019-10-G004903
Manuscript Type:	Engineering Note
Date Submitted by the Author:	20-Oct-2019
Complete List of Authors:	Zhang, Qingrui; Delft University of Technology, Liu, Hugh; University of Toronto, Institute for Aerospace Studies
Subject Index Category:	30900 Control System Design < 30000 GUIDANCE, CONTROL, AND DYNAMICS TECHNOLOGY, 32500 Navigation < 30000 GUIDANCE, CONTROL, AND DYNAMICS TECHNOLOGY, 30510 Autonomous Vehicles < 30000 GUIDANCE, CONTROL, AND DYNAMICS TECHNOLOGY

SCHOLARONE™
Manuscripts

Uncertainty and Disturbance Observer-Based Cooperative Formation Flight Control

Qingrui Zhang*

Delft University of Technology, Delft, 2628 CD, the Netherlands

Hugh H. T. Liu[†]

University of Toronto, Toronto, Ontario M3H 5T6, Canada

I. Introduction

A fixed-wing UAV flying in close formation, like migratory birds, can reduce their drag and save fuels almost as much as a well designed aerodynamically efficient UAV would bring [1, 2]. In spite of the benefits, close formation flight is challenging for UAV systems. According to [3], more than 30% of the maximum drag reduction will be lost, if the optimal relative position failed to be maintained within at least 10% wing span accuracy. The aerodynamic disturbances induced by trailing vortices of a leader UAV either endanger the flight stability of the follower UAV or frustrate close formation flight by deviating the follower UAV away from its optimal position. Certain cooperation mechanisms are expected to mitigate the performance degradation issue of the leader-follower architecture being applied to a large number of UAVs. Cooperative control coordinates multiple UAVs in terms of both their own states and the states of their neighbours [4, 5]. Different cooperative control strategies have been proposed, such as the potential field method [6], distance-based formation control [7, 8], behaviour-based control [9], virtual structure based control [10, 11], virtual leader-based control [12], etc.

Traditional potential field methods cannot secure an unique and unambiguous formation shape [6]. This drawback can be resolved by adding more constraints to the communication topology, thereby resulting in the so-called rigid formation and accordingly the distance-based formation control [4]. Construction of a rigid graph—the major concern for the distance-based formation control—will become formidable with the increase of vehicle amount. The distance-based control fails to account for formation rotation that is necessary for close formation at different flight maneuvers. The behaviour-based control defines several competing objectives, such as position tracking, collision avoidance, and formation holding [9, 13], but its stability is hard to analyze mathematically. An modification to the behaviour-based control is the virtual structure method [11]. The current virtual structure-based method was only applied to polygon formation, as it is too complex to describe a general formation shape. Another modification to the behaviour-based control is the virtual leader-based method which designs a virtual leader for each vehicle in formation. The virtual

---

*Post-doctoral fellow, Delft University of Technology; qingrui.zhang@mail.utoronto.ca, qingrui.zhang@tudelft.nl, Member AIAA (This work was done when I was working on my Ph.D. program at University of Toronto)

[†]Professor, University of Toronto Institute for Aerospace Studies; liu@utias.utoronto.ca, Associate Fellow AIAA

leader-based control will get more and more complicated to simultaneously describe the motions of all virtual leaders with the increase of the vehicle number.

This paper investigates the cooperative close formation control problem of a large number of UAVs. The existing research on close formation flight focuses on the case of two or three UAVs, so a leader-follower method is preferred due to its simplicity [14–21]. Different from existing research, we consider more than three UAVs in close formation flight, so a cooperative controller is more promising. Additionally, close formation flight requires all UAVs to fly in a "V-shape" formation in order to maximize the aerodynamic benefits. With the consideration of the merits and limits of different cooperative formation controllers, the virtual leader-based method is preferred for close formation flight. Since the simultaneous design of virtual leaders will be very complex for formation flight of a large number of UAVs, the virtual structure concept is borrowed in the design of virtual leaders. The entire formation is characterized as a rigid body. The desired formation trajectory is defined on the geometric center of the rigid body. The desired trajectory of a UAV is determined according to its required relative position to the formation center. The virtual leaders are obtained by passing all desired trajectories through certain cooperative filters which were employed to improve the transient performance. Based on the proposed cooperative controller, uncertainty and disturbance observers are introduced to estimate and compensate model uncertainties induced by trailing vortices. The proposed cooperative formation controller could at least ensure ultimate bounded control for formation tracking. If certain conditions are satisfied, asymptotic formation tracking control will be obtained. Major contributions of this paper lie in two aspects: 1) a robust cooperative controller is proposed for close formation flight of a large number of UAVs; 2) the difficulty in designing virtual leaders is resolved in terms of the virtual structure concept. Numerical simulations are presented to demonstrate the efficiency of the proposed design.

The rest of the paper is organized as follows. Section II formulates the major problem. Section III presents the virtual leader design. The robust cooperative control design is described in Section IV, while its stability is analyzed in Section V. Numerical simulations are reported in Section VI. Conclusions are given in Section VII.

II. Problem formulation

The cooperative formation controller in this paper focuses on the outer-loop control formation control. Assume the sideslip angle of a UAV is stabilized to be zero, while the angle of attack is kept to be small. A six-degree-of-freedom (6-DoF) nonlinear UAV model is used as given in (1).

$$
\begin{cases}
\dot{x}_i &= V_{Ti} \cos \gamma_i \cos \psi_i \\
\dot{y}_i &= V_{Ti} \cos \gamma_i \sin \psi_i \\
\dot{z}_i &= -V_{Ti} \sin \gamma_i
\end{cases}
\begin{cases}
\dot{V}_{Ti} &= \frac{T_i - D_i}{m_i} - g \sin \gamma_i + d_{Vi} \\
\dot{\gamma}_{ai} &= \frac{L_i \cos \mu_i}{m_i V_{Ti}} - \frac{g \cos \gamma_i}{V_{Ti}} + d_{\gamma i} \qquad (i \in \mathcal{V}) \\
\dot{\psi}_i &= \frac{L_i \sin \mu_i}{m_i V_{Ti} \cos \gamma_i} + d_{\psi i}
\end{cases}
\tag{1}
$$

where x_i, y_i, and z_i are the position coordinates of UAV i in the inertial frame (the north-east-down frame, NED), V_{Ti} is the total speed which is the resultant speed of the airspeed and the trailing vortex-induced wake velocity, γ_i and ψ_i are the flight path and course angles, respectively, m_i is the mass, g is the gravity acceleration, T_i is the engine thrust, L_i is the lift, D_i is the drag, μ_i is the bank angle, and d_{vi}, $d_{\gamma i}$, and $d_{\chi i}$ are lumped terms of model uncertainties and trailing vortex-induced disturbances with $d_{Vi} = -\frac{\Delta D_i}{m_i}$, $d_{\gamma i} = \frac{\Delta L_i \cos \mu_i - (Y_i + \Delta Y_i) \sin \mu_i}{m_i V_{Ti}}$, and $d_{\psi i} = \frac{\Delta L_i \sin \mu_i + (Y_i + \Delta Y_i) \cos \mu_i}{m_i V_{Ti} \cos \gamma_i}$, where ΔD_i, ΔL_i, and ΔY_i are trailing vortex-induced drag, lift and side force, respectively, and Y_i is the side force treated as a model uncertainty. Assume D_i is known, but it can be treated as unknown in real implementations. Additionally, γ_i is computed by $\sin \gamma_i = -\frac{\dot{z}_i}{V_{Ti}}$, while ψ_i is calculated according to $\tan \psi_i = \frac{\dot{y}_i}{\dot{x}_i}$. Control inputs for (1) are chosen to be T_i, α_i, and μ_i. Differentiating x_i, y_i, and z_i with respect to time twice yields

$$\ddot{x}_i = u_{xi} + d_{xi}, \qquad \ddot{y}_i = u_{yi} + d_{yi}, \qquad \ddot{z}_i = u_{zi} + d_{zi} \qquad (i \in \mathcal{V}) \tag{2}$$

where u_{xi}, u_{yi}, and u_{zi} are new control variables, and d_{xi}, d_{yi}, and d_{zi} are uncertainty and disturbance terms. We are interested in finding control laws for u_{xi}, u_{yi}, and u_{zi}, and the real control inputs T_i, L_i, and μ_i will be calculated using

$$\begin{cases} T_i & = & m_i u_{Vi} + m_i g \sin \gamma_i + D_i \\ L_i & = & \sqrt{\left(m_i V_{Ti} u_{yi} + m_i g \cos \gamma_i\right)^2 + \left(m_i V_{Ti} u_{\psi i} \cos \gamma_i\right)^2} \\ \mu_i & = & \tan^{-1}\left(\frac{m_i V_{Ti} u_{\psi i} \cos \gamma_i}{m_i V_{Ti} u_{yi} + m_i g \cos \gamma_i}\right) \end{cases} \tag{3}$$

where

$$\begin{cases} u_{Vi} & = & u_{xi} \cos \gamma_i \cos \psi_i + u_{yi} \cos \gamma_i \sin \psi_i - u_{zi} \sin \gamma_i \\ u_{\gamma i} & = & -\frac{u_{xi}}{V_{Ti}} \sin \gamma_i \cos \psi_i - \frac{u_{yi}}{V_{Ti}} \sin \gamma_i \sin \psi_i - \frac{u_{zi}}{V_{Ti}} \sin \gamma_i \\ u_{\psi i} & = & -\frac{u_{xi} \sin \psi_i}{V_{Ti} \cos \gamma_i} + \frac{u_{yi} \cos \psi_i}{V_{Ti} \cos \gamma_i} \end{cases} \tag{4}$$

The control input for α_i is obtained by $\alpha_i = \frac{L_i - L_{0i}}{L_{\alpha i}}$. Define $\mathbf{p}_i = [x_i, y_i, z_i]^T$, and we have
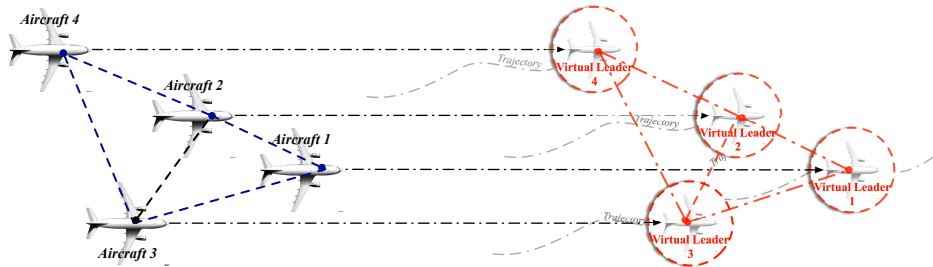

Figure 1   Virtual leader-based close formation flight control

$$\dot{\mathbf{p}}_i = \mathbf{v}_i, \qquad \dot{\mathbf{v}}_i = \mathbf{u}_i + \mathbf{d}_i \qquad (i \in \mathcal{V}) \tag{5}$$

3

where $\mathbf{v}_i = [\dot{x}_i, \dot{y}_i, \dot{z}_i]^T$ is the speed vector, $\mathbf{u}_i = \left[u_{xi}, u_{yi}, u_{zi}\right]^T$ is the control input vector, and $\mathbf{d}_i = \left[d_{xi}, d_{yi}, d_{zi}\right]^T$ is the model uncertainty and disturbance vector. The objective is to coordinate UAVs to track formation trajectories defined by a group of virtual leaders as shown in Figure 1. UAVs will share tracking errors with their neighbours. Let $\mathbf{r}_i$ be the position of the virtual leader i, and assume that both $\dot{\mathbf{r}}_i$ and $\ddot{\mathbf{r}}_i$ are available.

III. Cooperative motion planning

The communication topology among UAVs in close formation is modeled using an undirected graph $\mathscr{G}$ which is denoted by a triplet $\mathscr{G} := \{\mathscr{V}, \mathscr{E}, \mathcal{A}\}$ with a node set $\mathscr{V} = \{1, \ldots, n\}$, an edge set $\mathscr{E} \subseteq \mathscr{V} \times \mathscr{V}$, and an adjacency matrix $\mathcal{A} = \left[a_{ij}\right] \in \mathbb{R}^{n \times n}$ [22, 23]. Each node $i \in \mathscr{V}$ represents a UAV i in close formation. If a UAV i receives information from a UAV j ($j \neq i$), there is an edge $(i, j) \in \mathscr{E}$, and $a_{ij} = 1$. If $(i, j) \in \mathscr{E}$, UAV j is called an neighbour of UAV i. The neighbourhood of UAV i is denoted by $\mathscr{N}_i := \{\forall j \in \mathscr{V} \,|\, (i, i) \in \mathscr{E}\}$. In an undirected communication, $(j, i) \in \mathscr{E}$ implies $(i, j) \in \mathscr{E}$ and $a_{ij} = a_{ji} = 1$, whereas $a_{ij} = a_{ji} = 0$ if $(i,j) \notin \mathscr{E}$. Note that $(i, i) \notin \mathscr{E}$, $\forall i \in \mathscr{V}$, so $a_{ii} = 0$. The degree matrix of a graph $\mathscr{G}$ is a diagonal matrix $\mathcal{D} = diag \{d_1, \ldots, d_n\}$, where $d_i = \sum_{j=1}^n a_{ij}$, $\forall i \in \mathscr{V}$. The Laplacian matrix of $\mathscr{G}$ is defined to be $\mathcal{L} = \mathcal{D} - \mathcal{A}$. A path on $\mathscr{G}$ between i_1 and i_l is a sequence of edges of the form (i_j, i_{j+1}), where $j = 1, \ldots, l - 1$ and $i_j \in \mathscr{V}$. An undirected graph $\mathscr{G}$ is connected, if there exists a path from each node $i \in \mathscr{V}$ to any other nodes. An undirected graph $\mathscr{G}$ is connected, iff 0 is a simple eigenvalue of the Laplacian matrix $\mathcal{L}$ with the associate eigenvector $\mathbf{1}_n \in \mathbb{R}^{n \times 1}$ of all ones, while all the other eigenvalues are positive [24]. Assume the graph $\mathscr{G}$ is connected in this paper, so $\mathcal{L} \leq 0$ and $\mathcal{L}\mathbf{1}_n = \mathbf{0}$.

The challenge in a virtual leader-based method is to simultaneously design virtual leaders and make them keep the optimal formation shape under different maneuvers. Such a challenge will get much more difficult, when a large number of UAVs are considered in formation flight. In this paper, the virtual structure concept is employed, where desired formation shape is taken as a certain rigid body. The formation reference trajectory is described on the geometric center of the rigid body. As shown in Figure 2, desired motions for a UAV are defined using its relative position and motion to the geometric center of the rigid body. In Figure 2.a, $\mathbf{r}_i$ is the desired position vector of UAV i in the inertial frame, whereas $\mathbf{r}_c$ is the position vector of the formation center in the inertial frame. In close formation, all UAVs fly in the same altitude. Horizontal relative positions are constant in a local frame fixed to the formation center. Shown in Figure 2.b is the constant position vector $\boldsymbol{p}_{ri}$ of a virtual leader i in the local frame of the formation center, so one has

$$\begin{cases} \mathbf{r}_i & = \mathbf{r}_c + \underline{\mathbf{C}}_{BI}^T \left(\psi_c\right) \boldsymbol{p}_{ri} \\ \dot{\mathbf{r}}_i & = \dot{\mathbf{r}}_c + \underline{\dot{\mathbf{C}}}_{BI}^T \left(\psi_c\right) \boldsymbol{p}_{ri} = \dot{\mathbf{r}}_c + \underline{\mathbf{C}}_{BI}^T \left(\psi_c\right) \omega_c^\times \boldsymbol{p}_{ri} \\ \ddot{\mathbf{r}}_i & = \ddot{\mathbf{r}}_c + \underline{\mathbf{C}}_{BI}^T \left(\psi_c\right) \omega_c^\times \omega_c^\times \boldsymbol{p}_{ri} + \underline{\mathbf{C}}_{BI}^T \left(\psi_c\right) \dot{\omega}_c^\times \boldsymbol{p}_{ri} \end{cases} \tag{6}$$

(a) Motions in the inertial frame   (b) Positions in a local frame
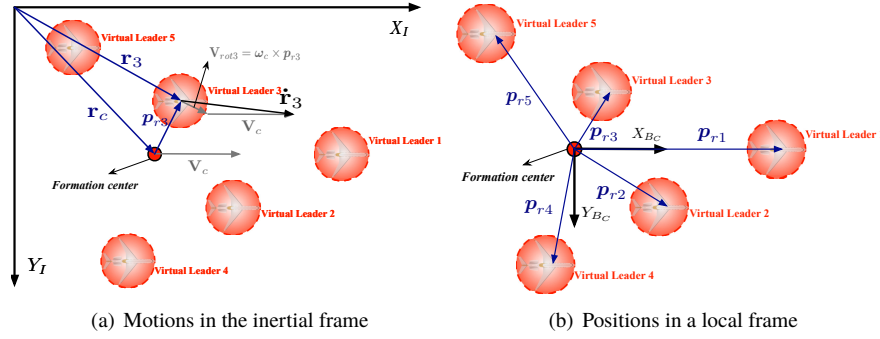
Figure 2   Motions and coordinates of virtual leaders

where $\mathbf{r}_c = [x_c, y_c, z_c]^T$, $\underline{\mathbf{C}}_{BI}(\psi_c)$ is a rotation matrix and $\omega_c^\times$ is a cross-product matrix.

$$\underline{\mathbf{C}}_{BI}(\psi_c) = \begin{bmatrix} \cos\psi_c & \sin\psi_c & 0 \\ -\sin\psi_c & \cos\psi_c & 0 \\ 0 & 0 & 1 \end{bmatrix}, \qquad \omega_c^\times = \begin{bmatrix} 0 & -\dot\psi c & 0 \\ \dot\psi c & 0 & 0 \\ 0 & 0 & 0 \end{bmatrix}$$

Although $\boldsymbol{p}_{ri}$ is assumed to be constant, our method can be extended to the case with time-varying $\boldsymbol{p}_{ri}$. Note that reference trajectories by (6) are not smooth, if there are any sudden changes in the accelerations of the formation center or angular rates of the local frame. If a UAV is initially far away from its designated reference position, dramatic control efforts will be needed, which might violates control constraints. Hence, instead of implementing (6) directly, a cooperative filter is introduced as given below for the i-th virtual leader ($\forall i \in \mathcal{V}$).

$$\begin{cases} \dot{\widehat{\mathbf{r}}}_i &= \widehat{\mathbf{v}}_i \\ \dot{\widehat{\mathbf{v}}}_i &= \ddot{\mathbf{r}}_i - \kappa_{\mathbf{p}}\widehat{\mathbf{e}}_{\mathbf{p}i} - \kappa_{\mathbf{v}}\widehat{\mathbf{e}}_{\mathbf{v}i} - \sum_{j \in \mathcal{N}_i}\left[c_{\mathbf{p}}\left(\widehat{\mathbf{e}}_{\mathbf{p}i} - \widehat{\mathbf{e}}_{\mathbf{p}j}\right) + c_{\mathbf{v}}\left(\widehat{\mathbf{e}}_{\mathbf{v}i} - \widehat{\mathbf{e}}_{\mathbf{v}j}\right) \right] \end{cases} \tag{7}$$

where $\widehat{\mathbf{r}}_i = [\widehat{x}_i, \widehat{y}_i, \widehat{z}_i]^T$ is the position vector in the inertial frame, $\widehat{\mathbf{v}}_i$ is the velocity vector, $\widehat{\mathbf{e}}_{\mathbf{p}i} = \widehat{\mathbf{r}}_i - \mathbf{r}_i$, $\widehat{\mathbf{e}}_{\mathbf{v}i} = \widehat{\mathbf{v}}_i - \mathbf{v}_i$, and $\kappa_{\mathbf{p}}$, $\kappa_{\mathbf{v}}$, $c_{\mathbf{p}}$, and $c_{\mathbf{v}}$ are diagonal positive definite gain matrices. From a motion planning perspective, the virtual structure is introduced to ensure rigid formation shape when reference motions are planned for all UAVs. The cooperative filter (7) is employed to smooth the planned motions in order to make them feasible and applicable. For any initial states $\widehat{\mathbf{r}}_i(t_0)$ and $\widehat{\mathbf{v}}_i(t_0)$, there exist $\widehat{\mathbf{r}}_i(t) \to \mathbf{r}_i(t)$ and $\widehat{\mathbf{v}}_i(t) \to \mathbf{v}_i(t)$ exponentially as $t \to \infty$, $\forall i \in \mathcal{V}$.

IV. Robust cooperative formation control

The general control law as shown in Figure 3 is expressed as

$$u_{\rho i} = u_{\rho 0 i} - \widehat{d}_{\rho i}, \qquad \rho \in \{x, y, z\} \qquad (i \in \mathcal{V}) \tag{8}$$

where $u_{\rho 0 i}$ is the baseline cooperative control, and $\widehat{d}_{\rho i}$ is the estimation of $d_{\rho i}$.
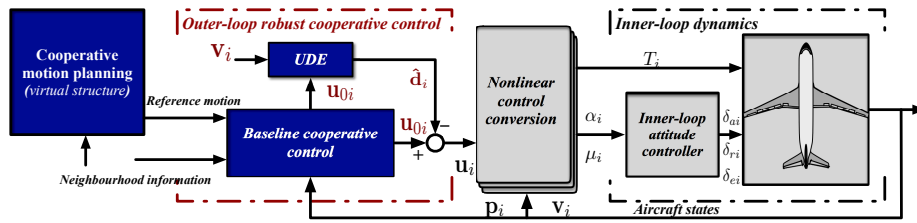
5

Figure 3   UDE-based robust cooperative formation control

A. Uncertainty and disturbance observer design

Assume that $u_{\rho i0}$ has been well designed to stabilize the nominal double integrator system (2) when $d_{\rho i} = 0$. Substituting (8) into (2) yields

$$\ddot{\rho}_i = u_{\rho 0 i} - \widehat{d}_{\rho i} + d_{\rho i}, \quad \rho \in \{x, y, z\} \tag{9}$$

In terms of results in [25–27], a stable low-pass filter $G_{\rho i}(s)$ is used to estimate $d_{\rho i}$, that is

$$G_{\rho i}(s) = \frac{1}{\mathcal{T}_{\rho i} s + 1}, \quad \rho \in \{x, y, z\} \tag{10}$$

where $\mathcal{T}_{\rho i}$ are time constants. Hence,

$$\widehat{d}_{\rho i} = \mathcal{L}^{-1}\left\{G_{\rho i}(s)\right\} * d_{\rho i}, \quad \rho \in \{x, y, z\} \tag{11}$$

where $\mathcal{L}^{-1}\{\cdot\}$ is the inverse Laplace transform and "$*$" denotes the convolution. Applying (11) to (9) yields

$$\ddot{\rho}_i = u_{\rho 0 i} + \mathcal{L}^{-1}\left\{1 - G_{\rho i}(s)\right\} * d_{\rho i}, \quad \rho \in \{x, y, z\} \tag{12}$$

where $1 - G_{\rho i}(s) = \frac{\mathcal{T}_{\rho i} s}{\mathcal{T}_{\rho i} s + 1}$ are high-pass filters. If the bandwidth of $G_{\rho i}(s)$ is chosen properly, the impact of $d_{\rho i}$ on the system can be ruled out. In terms of (9), we can denote $d_{\rho i}$ as a function of $\ddot{\rho}_i$, $u_{\rho 0 i}$, and $\widehat{d}_{\rho i}$. The following applicable uncertainty and disturbance observer is eventually obtained.

$$\widehat{d}_{\rho i} = \frac{1}{\mathcal{T}_{\rho i}}\left(\dot{\rho}_i(t) - \dot{\rho}_i(0) - \int_0^t u_{\rho 0 i} dt\right), \quad \rho \in \{x, y, z\} \tag{13}$$

B. Baseline cooperative control design

When being rewritten in a matrix form, the control law (8) is

$$\mathbf{u}_i = \mathbf{u}_{0i} - \widehat{\mathbf{d}}_i, \qquad (i \in \mathscr{V}) \tag{14}$$

Let $\mathbf{e}_{\mathbf{p}i} = \mathbf{p}_i - \tilde{\mathbf{r}}_i = \left[e_{xi}, e_{yi}, e_{zi} \right]^T$ and $\mathbf{e}_{\mathbf{v}i} = \mathbf{v}_i - \tilde{\mathbf{v}}_i = \left[e_{\dot{x}i}, e_{\dot{y}i}, e_{\dot{z}i} \right]^T$. The baseline cooperative control is

$$\mathbf{u}_{0i} = \ddot{\mathbf{r}}_i - K_p \mathbf{e}_{\mathbf{p}i} - K_v \mathbf{e}_{\mathbf{v}i} - \sum_{j \in \mathscr{N}_i} \left[C_p \left(\mathbf{e}_{\mathbf{p}i} - \mathbf{e}_{\mathbf{p}j} \right) + C_v \left(\mathbf{e}_{\mathbf{v}i} - \mathbf{e}_{\mathbf{v}j} \right) \right] \tag{15}$$

where $K_p \in \mathbb{R}^{3\times3}$, $K_v \in \mathbb{R}^{3\times3}$, $C_p \in \mathbb{R}^{3\times3}$, and $C_v \in \mathbb{R}^{3\times3}$ are all positive definite diagonal parameter matrices given by

$$K_p = diag \left\{ K_{px}, K_{py}, K_{pz} \right\}, \quad K_v = diag \left\{ K_{vx}, K_{vy}, K_{vz} \right\}$$
$$C_p = diag \left\{ C_{px}, C_{py}, C_{pz} \right\}, \quad C_v = diag \left\{ C_{vx}, C_{vy}, C_{vz} \right\}$$

Note that the same set of control gains are chosen, as we consider multiple homogeneous UAV models in close formation flight. Define $\widetilde{d}_{\rho i} = \widehat{d}_{\rho i} - d_{\rho i}$ as approximation errors. When substituting (15) and (14) into (5), one has

$$\begin{aligned}
\dot{\mathbf{e}}_{\mathbf{v}i} &= -K_p \mathbf{e}_{\mathbf{p}i} - K_v \mathbf{e}_{\mathbf{v}i} - \sum_{j \in \mathscr{N}_i} a_{ij} \left[C_p \left(\mathbf{e}_{\mathbf{p}i} - \mathbf{e}_{\mathbf{p}j} \right) + C_v \left(\mathbf{e}_{\mathbf{v}i} - \mathbf{e}_{\mathbf{v}j} \right) \right] \\
&\quad + \kappa_p \widehat{\mathbf{e}}_{\mathbf{p}i} + \kappa_v \widehat{\mathbf{e}}_{\mathbf{v}i} + \sum_{j \in \mathscr{N}_i} \left[c_p \left(\widehat{\mathbf{e}}_{\mathbf{p}i} - \widehat{\mathbf{e}}_{\mathbf{p}j} \right) + c_v \left(\widehat{\mathbf{e}}_{\mathbf{v}i} - \widehat{\mathbf{e}}_{\mathbf{v}j} \right) \right] - \widetilde{\mathbf{d}}_i
\end{aligned} \tag{16}$$

where $\widetilde{\mathbf{d}}_i = \left[\widetilde{d}_{xi}, \widetilde{d}_{yi}, \widetilde{d}_{zi} \right]^T$. Let $\mathbf{e}_{\mathbf{p}} = \left[\mathbf{e}_{\mathbf{p}1}^T, \ldots, \mathbf{e}_{\mathbf{p}n}^T \right]^T$, $\mathbf{e}_{\mathbf{v}} = \left[\mathbf{e}_{\mathbf{v}1}^T, \ldots, \mathbf{e}_{\mathbf{v}n}^T \right]^T$, and $\widetilde{\mathbf{d}} = \left[\widetilde{\mathbf{d}}_1^T, \ldots, \widetilde{\mathbf{d}}_n^T \right]^T$. The closed-loop tracking error dynamics are

$$\begin{aligned}
\dot{\mathbf{e}}_{\mathbf{v}} &= - \left(\mathbf{I}_n \otimes K_p + \mathcal{L} \otimes C_p \right) \mathbf{e}_{\mathbf{p}} - \left(\mathbf{I}_n \otimes K_v + \mathcal{L} \otimes C_v \right) \mathbf{e}_{\mathbf{v}} + \left(\mathbf{I}_n \otimes \kappa_{\mathbf{p}} + \mathcal{L} \otimes c_{\mathbf{p}} \right) \widehat{\mathbf{e}}_{\mathbf{p}} \\
&\quad + \left(\mathbf{I}_n \otimes \kappa_{\mathbf{v}} + \mathcal{L} \otimes c_{\mathbf{v}} \right) \widehat{\mathbf{e}}_{\mathbf{v}} - \widetilde{\mathbf{d}}
\end{aligned} \tag{17}$$

where $\mathbf{I}_n \in \mathbb{R}^{n\times n}$ is an identity matrix.

V. Stability analysis

The stability analysis is divided into two steps. At the first step, it is shown that the nominal system of (17) without the consideration of uncertainties and disturbances can be stabilized by the baseline cooperative controller (15). Once the nominal system is stabilized, the uncertainty and disturbance observer design will be validated and the estimation errors will be ensured to be uniformly and ultimately bounded. The closed-loop stability of (17) is analyzed at the second step.

Assuming $\widetilde{\mathbf{d}}_i = \mathbf{0}$ yields the following nominal tracking error dynamics.

$$\dot{\mathbf{e}}_{\mathbf{v}} = - \left(\mathbf{I}_n \otimes K_p + \mathcal{L} \otimes C_p \right) \mathbf{e}_{\mathbf{p}} - \left(\mathbf{I}_n \otimes K_v + \mathcal{L} \otimes C_v \right) \mathbf{e}_{\mathbf{v}} + \sigma_{\widehat{\mathbf{e}}} \tag{18}$$

where $\sigma_{\widehat{\mathbf{e}}} = \left(\mathbf{I}_n \otimes \boldsymbol{\kappa}_{\mathbf{p}} + \mathcal{L} \otimes \boldsymbol{c}_{\mathbf{p}}\right) \widehat{\mathbf{e}}_{\mathbf{p}} + \left(\mathbf{I}_n \otimes \boldsymbol{\kappa}_{\mathbf{v}} + \mathcal{L} \otimes \boldsymbol{c}_{\mathbf{v}}\right) \widehat{\mathbf{e}}_{\mathbf{v}}$. The tracking errors of the cooperative filter (7), $\widehat{\mathbf{e}}_{\mathbf{p}}$ and $\widehat{\mathbf{e}}_{\mathbf{v}}$, converge to zero ~~exponentially,~~ so $\lim_{t\to\infty} \sigma_{\widehat{\mathbf{e}}} \to \mathbf{0}$ exponentially. If (18) is input-to-state stable with respect to $\sigma_{\widehat{\mathbf{e}}}$, the nominal system will be asymptotically stable by Lemma 4.7 in [28].

The Laplacian matrix $\mathcal{L}$ is a real symmetric matrix, so it can be diagonalized by an orthogonal constant matrix. Let $\boldsymbol{Q} = [\boldsymbol{Q}_1, \ldots, \boldsymbol{Q}_n] \in \mathbb{R}^{n \times n}$ be an orthogonal matrix such that $\boldsymbol{Q}^T \mathcal{L} \boldsymbol{Q} = \boldsymbol{\Lambda}$ where $\boldsymbol{\Lambda} = diag\{\lambda_1, \ldots, \lambda_n\}$. Choosing $\boldsymbol{Q}_1 = \frac{1}{\sqrt{n}} \mathbf{1}_n$ yields $\lambda_1 = 0$ and $\boldsymbol{\Lambda} = diag\left\{0, \bar{\boldsymbol{Q}}^T \mathcal{L} \bar{\boldsymbol{Q}}\right\} = diag\left\{0, \bar{\boldsymbol{\Lambda}}\right\}$, where $\bar{\boldsymbol{Q}} = [\boldsymbol{Q}_2, \ldots, \boldsymbol{Q}_n] \in \mathbb{R}^{n \times (n-1)}$ and $\bar{\boldsymbol{\Lambda}} = diag\{\lambda_2, \lambda_3, \ldots, \lambda_n\} > 0$ with $\lambda_2, \lambda_3, \ldots, \lambda_n$ denoting positive eigenvalues of $\mathcal{L}$. In terms of $\boldsymbol{Q}$, $\mathbf{e}_{\mathbf{p}}$ and $\mathbf{e}_{\mathbf{v}}$ are transformed into a new coordinate system — that is, $\boldsymbol{\varepsilon}_{\boldsymbol{p}} = \left(\boldsymbol{Q}^T \otimes \mathbf{I}_3\right) \mathbf{e}_{\mathbf{p}} = \left[\boldsymbol{\varepsilon}_{\boldsymbol{p}1}^T, \boldsymbol{\varepsilon}_{\boldsymbol{p}2}^T, \ldots, \boldsymbol{\varepsilon}_{\boldsymbol{p}n}^T\right]^T$ and $\boldsymbol{\varepsilon}_{\boldsymbol{v}} = \left(\boldsymbol{Q}^T \otimes \mathbf{I}_3\right) \mathbf{e}_{\mathbf{v}} = \left[\boldsymbol{\varepsilon}_{\boldsymbol{v}1}^T, \boldsymbol{\varepsilon}_{\boldsymbol{v}2}^T, \ldots, \boldsymbol{\varepsilon}_{\boldsymbol{v}n}^T\right]^T$, where $\boldsymbol{\varepsilon}_{\boldsymbol{p}i} = \left[\varepsilon_{pxi}, \varepsilon_{pyi}, \varepsilon_{pzi}\right]^T \in \mathbb{R}^{3 \times 1}$ and $\boldsymbol{\varepsilon}_{\boldsymbol{v}i} = \left[\varepsilon_{vxi}, \varepsilon_{vyi}, \varepsilon_{vzi}\right]^T \in \mathbb{R}^{3 \times 1}$ with $i \in \mathcal{V}$. Note that $\boldsymbol{Q}^T \otimes \mathbf{I}_3$ is invertible, as both $\boldsymbol{Q}$ and $\mathbf{I}_3$ are non-singular. Hence,

$$\|\mathbf{e}_{\mathbf{p}}\|_2 \leq \|\left(\boldsymbol{Q} \otimes \mathbf{I}_3\right)\|_2 \|\boldsymbol{\varepsilon}_{\boldsymbol{p}}\|_2 = \|\boldsymbol{\varepsilon}_{\boldsymbol{p}}\|_2, \qquad \|\mathbf{e}_{\mathbf{v}}\|_2 \leq \|\left(\boldsymbol{Q} \otimes \mathbf{I}_3\right)\|_2 \|\boldsymbol{\varepsilon}_{\boldsymbol{v}}\|_2 = \|\boldsymbol{\varepsilon}_{\boldsymbol{v}}\|_2 \qquad \forall t > 0 \qquad (19)$$

Based on the coordinate transformation by $\boldsymbol{Q}^T \otimes \mathbf{I}_3$ and (18), one could get

$$\dot{\boldsymbol{\varepsilon}}_{\boldsymbol{v}} = -\left(\mathbf{I}_n \otimes \boldsymbol{K}_{\boldsymbol{p}} + \boldsymbol{\Lambda} \otimes \boldsymbol{C}_{\boldsymbol{p}}\right) \boldsymbol{\varepsilon}_{\boldsymbol{p}} - \left(\mathbf{I}_n \otimes \boldsymbol{K}_{\boldsymbol{v}} + \boldsymbol{\Lambda} \otimes \boldsymbol{C}_{\boldsymbol{v}}\right) \boldsymbol{\varepsilon}_{\boldsymbol{v}} + \bar{\sigma}_{\widehat{\mathbf{e}}} \qquad (20)$$

where $\bar{\sigma}_{\widehat{\mathbf{e}}} = \left(\boldsymbol{Q}^T \otimes \mathbf{I}_3\right) \sigma_{\widehat{\mathbf{e}}} = \left[\bar{\sigma}_1^T, \ldots, \bar{\sigma}_n^T\right]^T$ with $\bar{\sigma}_i = \left[\bar{\sigma}_{xi}, \bar{\sigma}_{yi}, \bar{\sigma}_{zi}\right]^T$ for $i = 1, 2, \ldots, n$. Since $\boldsymbol{Q}$ is nonsingular and $\lim_{t\to\infty} \sigma_{\widehat{\mathbf{e}}} \to \mathbf{0}$, one has $\lim_{t\to\infty} \bar{\sigma}_{\widehat{\mathbf{e}}} \to \mathbf{0}$. The dynamics of $\boldsymbol{\varepsilon}_{\boldsymbol{v}}$ is decoupled, as $\boldsymbol{K}_{\boldsymbol{p}}, \boldsymbol{K}_{\boldsymbol{v}}, \boldsymbol{K}_{\boldsymbol{p}}, \boldsymbol{C}_{\boldsymbol{v}}$, and $\boldsymbol{\Lambda}$ are all diagonal matrices. Therefore, we have

$$\begin{bmatrix} \dot{\varepsilon}_{\boldsymbol{p}\rho i} \\ \dot{\varepsilon}_{\boldsymbol{v}\rho i} \end{bmatrix} = \underbrace{\begin{bmatrix} 0 & 1 \\ -K_{\boldsymbol{p}\rho} - \lambda_i C_{\boldsymbol{p}\rho} & -K_{\boldsymbol{v}\rho} - \lambda_i C_{\boldsymbol{v}\rho} \end{bmatrix}}_{\mathbf{A}_{\rho i}} \begin{bmatrix} \varepsilon_{\boldsymbol{p}\rho i} \\ \varepsilon_{\boldsymbol{v}\rho i} \end{bmatrix} + \begin{bmatrix} 0 \\ \bar{\sigma}_{\rho i} \end{bmatrix} \qquad (21)$$

where $\rho \in \{x, y, z\}$ and $i \in \mathcal{V}$. Since $K_{\boldsymbol{p}\rho}, C_{\boldsymbol{p}\rho}, K_{\boldsymbol{v}\rho}, C_{\boldsymbol{v}\rho} > 0$, and $\lambda_i \geq 0$, $\mathbf{A}_{\rho i}$ are Hurwitz ($\forall \rho \in \{x, y, z\}$ and $\forall i \in \mathcal{V}$), so the system (21) is input-to-state stable with respect to $\bar{\sigma}_{\rho i}$ according to Lemma 4.7 in [28]. In terms of $\lim_{t\to\infty} \bar{\sigma}_{\widehat{\mathbf{e}}} \to \mathbf{0}$ and Lemma 4.7 in [28], the nominal system (21) is asymptotically stable, which implies the nominal system (18) is asymptotically stable. Let $\mathbf{e} = \left[\mathbf{e_p}^T, \mathbf{e_v}^T\right]^T$. The tracking error system (17) could be rewritten as

$$\dot{\mathbf{e}} = \underbrace{\begin{bmatrix} \mathbf{0} & \mathbf{I}_n \otimes \mathbf{I}_3 \\ -\mathbf{I}_n \otimes \boldsymbol{K}_{\boldsymbol{p}} - \mathcal{L} \otimes \boldsymbol{C}_{\boldsymbol{p}} & -\mathbf{I}_n \otimes \boldsymbol{K}_{\boldsymbol{v}} - \mathcal{L} \otimes \boldsymbol{C}_{\boldsymbol{v}} \end{bmatrix}}_{\mathbf{A}} \mathbf{e} + \underbrace{\begin{bmatrix} \mathbf{0} \\ -\mathbf{I}_n \otimes \mathbf{I}_3 \end{bmatrix}}_{\mathbf{B}} \left(\widetilde{\mathbf{d}} - \sigma_{\widehat{\mathbf{e}}}\right) \qquad (22)$$

where $\mathbf{A}$ is Hurwitz, as the nominal system is asymptotically stable. Let $\widehat{\mathbf{e}} = \left[\widehat{\mathbf{e}}_{\mathbf{p}}^T, \widehat{\mathbf{e}}_{\mathbf{v}}^T\right]^T$ be the tracking error vector of

the command filter (7), so

$$\dot{\widehat{\mathbf{e}}} = \underbrace{\begin{bmatrix} \mathbf{0} & \mathbf{I}_n \otimes \mathbf{I}_3 \\ -\mathbf{I}_n \otimes \boldsymbol{\kappa}_\mathbf{p} - \mathcal{L} \otimes c_\mathbf{p} & -\mathbf{I}_n \otimes \boldsymbol{\kappa}_\mathbf{v} - \mathcal{L} \otimes c_\mathbf{v} \end{bmatrix}}_{\mathbf{A}_{\widehat{\mathbf{e}}}} \widehat{\mathbf{e}}$$
(23)

where $\mathbf{A}_{\widehat{\mathbf{e}}}$ is Hurwitz. It is easy to obtain that $\sigma_{\widehat{\mathbf{e}}} = \mathbf{B}^T \mathbf{A}_{\widehat{\mathbf{e}}} \widehat{\mathbf{e}}$. Define

$$\mathbf{A}_\mathbf{d} = diag \left\{ -1/\mathcal{T}_{x1}, \ -1/\mathcal{T}_{y1}, \ -1/\mathcal{T}_{z1}, \ \dots, \ -1/\mathcal{T}_{xn}, \ -1/\mathcal{T}_{yn}, \ -1/\mathcal{T}_{zn} \right\}$$

where $\mathbf{A}_\mathbf{d}$ is Hurwitz. The following error dynamic model can be obtained for the uncertainty and disturbance observers.

$$\dot{\widetilde{\mathbf{d}}} = \mathbf{A}_\mathbf{d} \widetilde{\mathbf{d}} - \dot{\mathbf{d}}$$
(24)

Define $\mathbf{e}_\mathbf{a} = \begin{bmatrix} \mathbf{e}^T, \widehat{\mathbf{e}}^T, \widetilde{\mathbf{d}}^T \end{bmatrix}^T$. The composite error system by (22) and (24) is

$$\dot{\mathbf{e}}_a = \underbrace{\begin{bmatrix} \mathbf{A} & -\mathbf{B}\mathbf{B}^T \mathbf{A}_{\widehat{\mathbf{e}}} & \mathbf{B} \\ \mathbf{0} & \mathbf{A}_{\widehat{\mathbf{e}}} & \mathbf{0} \\ \mathbf{0} & \mathbf{0} & \mathbf{A}_\mathbf{d} \end{bmatrix}}_{\mathbf{A}_\mathbf{a}} \mathbf{e}_\mathbf{a} + \underbrace{\begin{bmatrix} \mathbf{0} \\ \mathbf{0} \\ -\mathbf{I}_n \otimes \mathbf{I}_3 \end{bmatrix}}_{\mathbf{B}_\mathbf{a}} \dot{\mathbf{d}}$$
(25)

where $\mathbf{A}_\mathbf{a}$ is Hurwitz, as $\mathbf{A}$, $\mathbf{A}_{\widehat{\mathbf{e}}}$, and $\mathbf{A}_\mathbf{d}$ are all Hurwitz. The system (25) is input-to-state stable with respect to $\dot{\mathbf{d}}$, which implies that (17) is input-to-state stable with respect to $\dot{\mathbf{d}}$.

Theorem 1 *Suppose Assumption ?? holds. The closed-loop close formation tracking error system (17) with the uncertainty and disturbance observer (13) is input-to-state stable with respect to $\dot{\mathbf{d}} = \begin{bmatrix} \dot{\mathbf{d}}_1^T, \ \dots, \ \dot{\mathbf{d}}_n^T \end{bmatrix}^T$ where $\dot{\mathbf{d}}_i = \begin{bmatrix} \dot{d}_{xi}, \dot{d}_{yi}, \dot{d}_{zi} \end{bmatrix}^T$.*

VI. Numerical simulations

This section presents numerical simulation results which demonstrate the efficiency of the proposed virtual leader-based robust cooperative formation controller for close formation flight. A group of virtual leaders are introduced, where each virtual leader will provide reference signals for a corresponding UAV in close formation as shown in Figure 1. In the numerical simulations, the close formation flight problem of five UAVs is considered, namely $\mathcal{V} = \{1, 2, 3, 4, 5\}$. Necessary UAV parameters are given in Table 1. The formation aerodynamic disturbances are assumed to be unknown and generated using the aerodynamic model presented by [3].

Table 1   UAV parameters

Parameter	Wing area (m^2)	Wing span (m)	Mass (kg)	Drag coefficient
Value	27.87	9.144	9295.44	0.0794

According to the aerodynamic analysis in [3], the optimal formation shape for close formation flight of five UAVs is given in Figure 4.a. All UAVs are required to fly at the same altitude, and the optimal horizontal relative positions between two UAVs are defined in the body frame of the first virtual leader as shown in Figure 4.a. The communication topology is illustrated in Figure 4.b with the adjacency matrix and degree matrix given in (26). For any UAV i and j with $i, j \in \mathcal{V}$ and $i \neq j$, if there is a connection between them in Figure 4.b, it implies that aicraft i and j are able to communicate with each other, and meanwhile $a_{ij} = 1$, otherwise, $a_{ij} = 0$.

$$\mathcal{A} = \begin{bmatrix} 0 & 1 & 1 & 0 & 0 \\ 1 & 0 & 1 & 1 & 0 \\ 1 & 1 & 0 & 1 & 1 \\ 0 & 1 & 1 & 0 & 1 \\ 0 & 0 & 1 & 1 & 0 \end{bmatrix} \qquad \mathcal{D} = \begin{bmatrix} 2 & 0 & 0 & 0 & 0 \\ 0 & 3 & 0 & 0 & 0 \\ 0 & 0 & 4 & 0 & 0 \\ 0 & 0 & 0 & 3 & 0 \\ 0 & 0 & 0 & 0 & 2 \end{bmatrix} \qquad (26)$$

(a) The optimal formation shape   (b) Communication topology
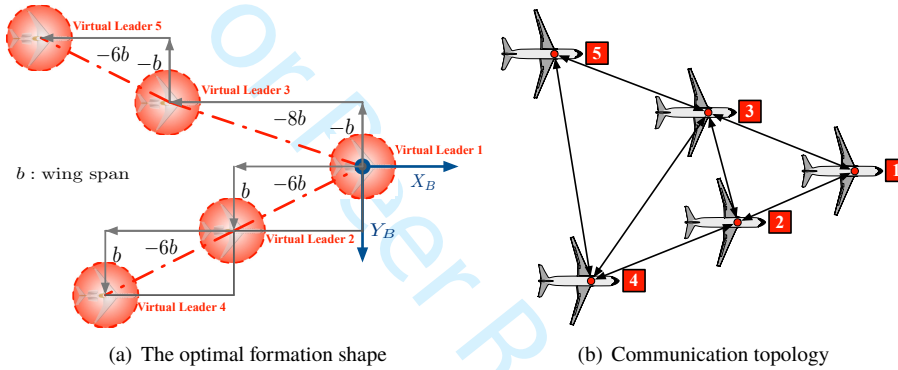
Figure 4   Virtual leader-based cooperative control

If we treat the optimal formation shape in Figure 4.a as a rigid body, the motion of each virtual leader could in general be resolved into a rotational motion around the formation geometric center and a translational motion which is equal to the translational motion of the formation center as shown in Figure 2.a. The formation trajectory is introduced on the formation geometric center and described using the following navigation model.

$$\dot{x}_c = V_c \cos \gamma_c \cos \psi_c, \quad \dot{y}_c = V_c, \cos \gamma_c \sin \psi_c, \quad \dot{z}_c = -V_c \sin \gamma_c, \quad \dot{V}_c = a_{Vc}, \quad \dot{\gamma}_c = a_{\gamma c}, \quad \dot{\psi}_c = a_{\psi c} \quad (27)$$

where x_c, y_c, and z_c represent the position coordinates of the optimal formation center in the inertial frame, V_c, γ_c, and ψ_c denote the ground velocity, flight path angle, and heading angle, respectively, and a_{Vc}, $a_{\gamma c}$, and $a_{\psi c}$ specify the acceleration, flight path angular rate, and heading angular rate, respectively.

The navigation model (27) describes the motion of the geometric centre of the optimal formation shape shown in Figure 4.a. The motion of all virtual leaders are calculated based on the motion of the geometric centre given in (27). Let $\boldsymbol{p}_{ri}$ be the position vector of the i-th virtual leader in the body frame of the navigation model of the geometric centre as shown in Figure 2.b. According to Figure 4.a, we have $\boldsymbol{p}_{r1} = [8b, 0, 0]^T$, $\boldsymbol{p}_{r2} = [2b, b, 0]^T$, $\boldsymbol{p}_{r3} = [0, -b, 0]^T$,

Table 2   Initial conditions

UAV	Position (m)			V_T (m/s)	γ (rad)	ψ (rad)
#	x	y	z			
1	190	190	-5005	121	0	0
2	155	215	-5015	116	0	0
3	140	182	-5005	115	0	$\frac{\pi}{120}$
4	85	225	-5015	119	0	0
5	65	172	-5015	120	0	$\frac{\pi}{100}$

$\boldsymbol{p}_{r4} = [-4b, 2b, 0]^T$, and $\boldsymbol{p}_{r5} = [-6b, -b, 0]^T$.

Initially, $x_c(0) = 26.87\ m$, $y_c(0) = 200\ m$, $z_c(0) = -5000\ m$, $V_c(0) = 120\ m/s$, and $\gamma_c(0) = \psi_c(0) = 0\ rad$.

The acceleration is zero, namely $a_{Vc} = 0$, while angular rate signals are

$$a_{\gamma c} = \begin{cases} \frac{\pi}{60} & 10 < t \le 45 \\ -\frac{\pi}{60} & 45 < t \le 80 \\ 0 & otherwise \end{cases}, \qquad a_{\psi c} = \begin{cases} \frac{\pi}{1080} & 10 < t \le 40 \\ -\frac{\pi}{1080} & 50 < t \le 80 \\ 0 & otherwise \end{cases} \qquad (28)$$

Cooperative filter gains are $\boldsymbol{\kappa_p} = diag\{1, 1, 1\}$, $\boldsymbol{\kappa_v} = diag\{2.5, 2.5, 2.5\}$, $\boldsymbol{c_v} = diag\{0.5, 0.5, 0.5\}$, and $\boldsymbol{c_p} = diag\{1.25, 1.25, 1.25\}$.
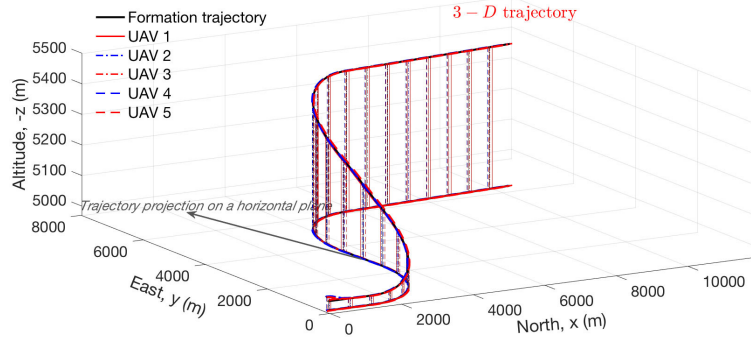
Figure 5   Trajectories of all five UAVs

The initial conditions of the five UAVs are listed in Table 2, while the same group of initial conditions are chosen for the cooperative filters. At the beginning all UAV is at level and straight flight with the original thrust $T_0 = 16954$ N. The same time constants are chosen for the uncertainty and disturbance observers of all UAVs, namely $\mathcal{T}_{\rho i} = 0.2$ s with $\rho \in \{x, y, z\}$ and $i \in \mathcal{V}$. The baseline control parameters are given in Table 3. The trajectory tracking responses of the five UAVs are shown in Figure 5, while the UAV trajectories at four crucial time periods are highlighted in Figure 6. Position tracking error responses are illustrated in Figures 7, 8 and 9, respectively, while the velocity tracking errors are presented in Figures 10, 11 and 12, respectively. The corresponding control inputs are given in Figures 13, 14 and 15. Close formation flight tracking is achieved by the proposed virtual-leader based robust cooperative control.

As indicated in Figures 10-12, oscillations are observed when $t = 10$ s, 40 s, and 80 s. It is because the

Table 3   Control parameters

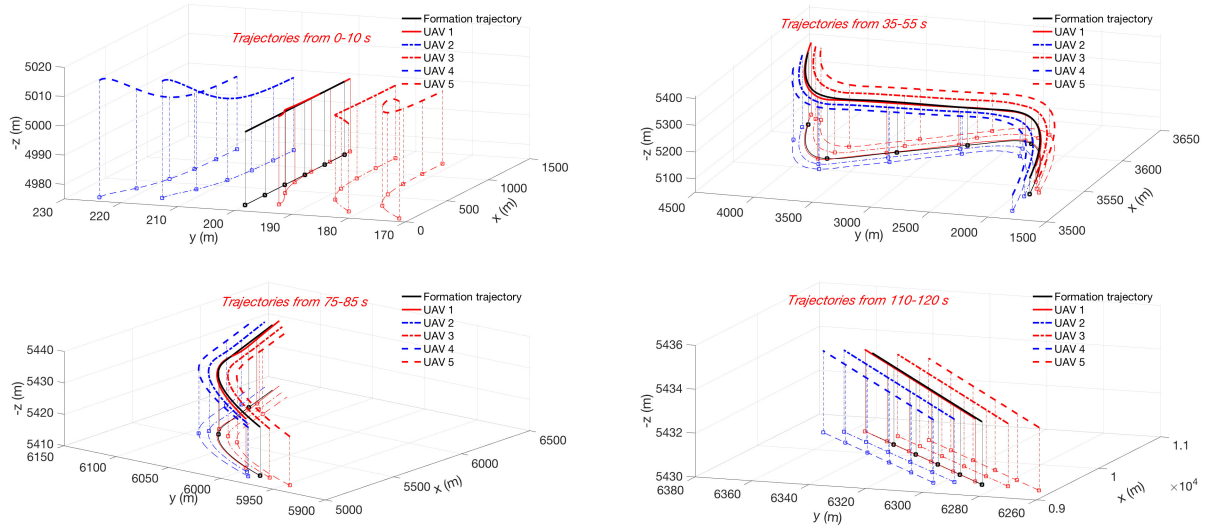| Parameters	K_{px}	K_{py}	K_{pz}	K_{vx}	K_{vy}	K_{vz}	C_{px}	C_{py}	C_{pz}	C_{vx}	C_{vy}	C_{vz}
Value	0.25	0.4	0.3	1.5	1.75	1.75	0.15	0.15	0.15	0.55	0.55	0.55

Figure 6   UAV trajectories at different time periods

reference trajectory signals are not smooth enough. According to (28), the angular rate signals $a_{\gamma c}$ and $a_{\chi c}$ have sudden changes at t = 10 s, 40 s, and 80 s. The real acceleration of each virtual leader should be $\ddot{\mathbf{r}}_i = \ddot{\mathbf{r}}_c + \underline{\mathbf{C}}_{WI}^T (\psi_c) \, \omega_c^\times \omega_c^\times \mathbf{p}_{ri} + \underline{\mathbf{C}}_{WI}^T (\psi_c) \, \dot{\mathbf{\Omega}}_c^\times \mathbf{p}_{ri}$ where the third term $\underline{\mathbf{C}}_{WI}^T (\psi_c) \, \dot{\mathbf{\Omega}}_c^\times \mathbf{p}_{ri}$ represents the impact of changes in the angular rates of the reference trajectories. However, $a_{\gamma c}$ and $a_{\chi c}$ are not changed smoothly, so $\underline{\mathbf{C}}_{WI}^T (\psi_c) \, \dot{\mathbf{\Omega}}_c^\times \mathbf{p}_{ri}$ will be infinity at t = 10 s, 40 s, and 80 s. In order to avoid this infinity issue, the acceleration of each virtual leader is estimated by $\ddot{\mathbf{r}}_i = \ddot{\mathbf{r}}_c + \underline{\mathbf{C}}_{WI}^T (\psi_c) \, \omega_c^\times \omega_c^\times \mathbf{p}_{ri}$. Therefore, accelerations of all virtual leaders are underestimated at t = 10 s, 40 s, and 80 s, which results in the oscillations in the responses.

When in close formation flight, the very first UAV (UAV 1 in the simulations) is not flying at any trailing vortices of other UAV, so it is the only UAV which doesn't receive any aerodynamic benefits. The first UAV has the same performance as a UAV at solo flight with the same conditions. Therefore, it could be used as an benchmark to show the benefits of close formation flight. In comparison with UAV 1, other UAV could experience at least 5.5% decrease in their thrust inputs in close formation flight as shown in Figure 13. Hence, close formation flight could help follower UAVs to reduce their drag and eventually help to save energies.

VII. Conclusions

The paper investigated the robust cooperative control for fixed-wing UAVs in close formation flight to save energy. A novel cooperative close formation controller was proposed by combining the virtual structure method and the virtual
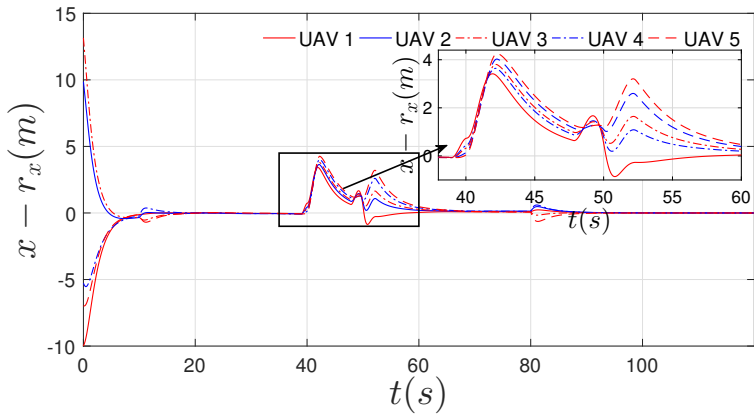
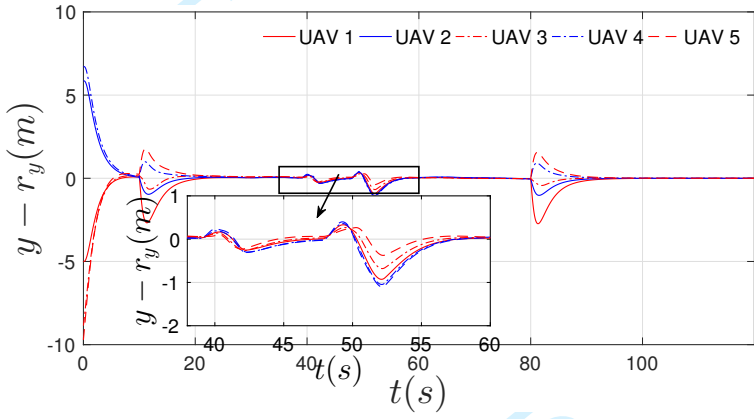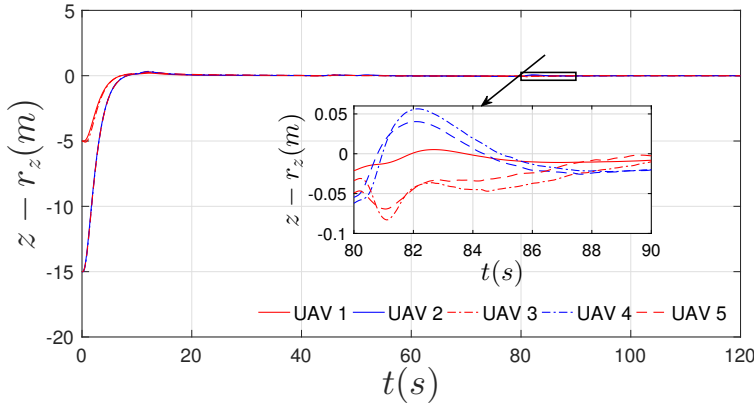Figure 7   Longitudinal position tracking errors

Figure 8   Lateral position tracking errors

Figure 9   Vertical position tracking errors

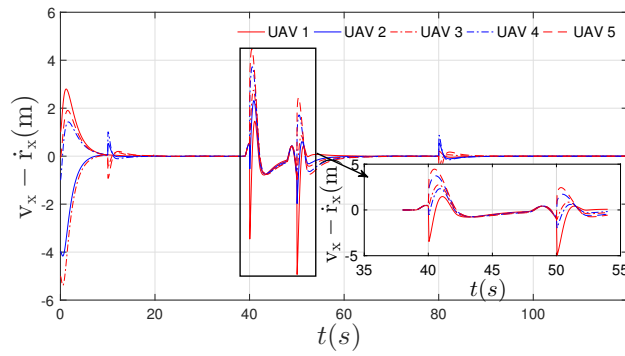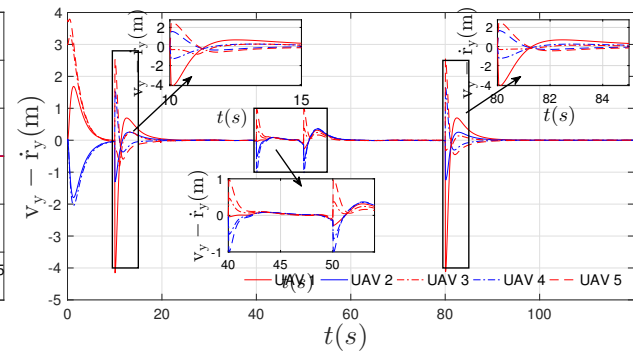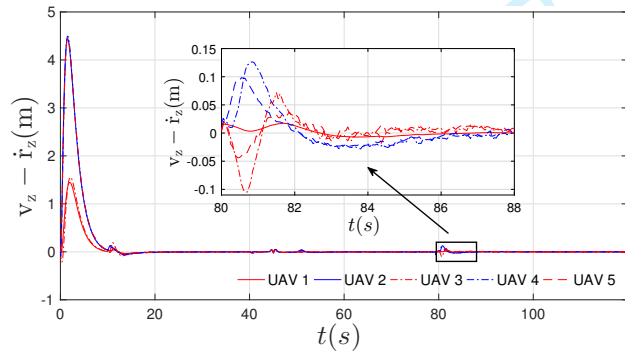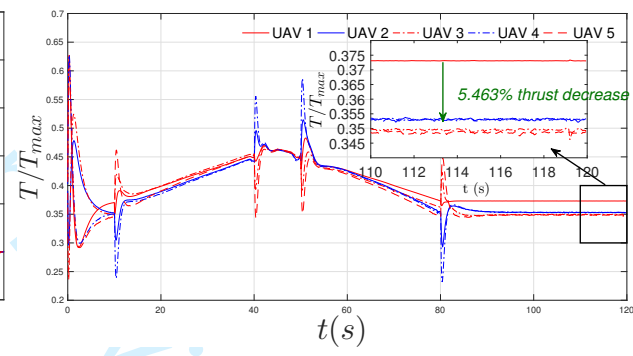Figure 10   Velocity errors in X_I axis

Figure 11   Velocity errors in Y_I axis

Figure 12   Velocity errors in Z_I axis
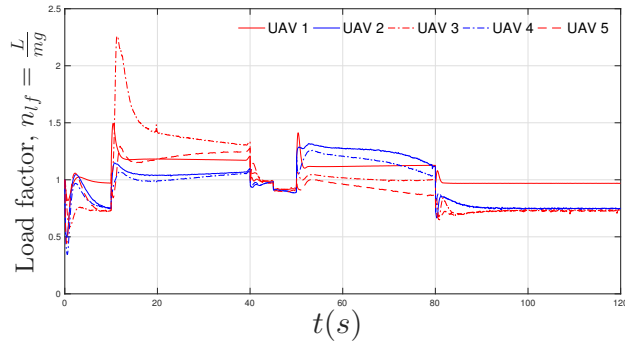

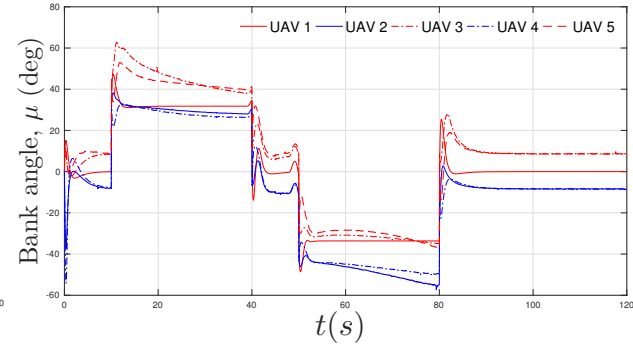Figure 13   Thrust inputs

Figure 14   Load factors

Figure 15   Bank angle inputs

14

leader-based control method. The virtual structure method was introduced to describe the desired trajectories of UAVs in close formation flight. The desired trajectories were passed through a group of cooperative filters to produce the motions of virtual leaders. UAVs in close formation flight were required to track the motions of their designated virtual leaders. The model uncertainties induced by trailing vortices of other UAV were estimated and compensated by using uncertainty and disturbance observers. The analysis has shown that the states of the virtual leaders will exponentially converge to the desired formation trajectories, while the proposed robust cooperative close formation controller could at least ensure bounded close formation tracking performance. Numerical simulations on close formation flight of five UAVs were performed to show the efficiency of the proposed design.

References

[1] Pahle, J., Berger, D., Venti, M., Duggan, C., Faber, J., and Cardinal6, K., "An Initial Flight Investigation of Formation Flight for Drag Reduction on the C-17 Aircraft," *Proceedings of 2012 Atmospheric Flight Mechanics Conference, AIAA AVIATION Forum*, AIAA, Minneapolis, Minnesota, USA, 2012. doi:10.2514/6.2012-4802, AIAA 2012-4802.

[2] Bieniawski, S. R., Clark, R. W., Rosenzweig, S. E., and Blake, W. B., "Summary of Flight Testing and Results for the Formation Flight for Aerodynamic Benefit Progam," *Proceedings of 52nd AIAA Aerospace Sciences Meeting*, AIAA, National Harbor, MD, 2014. doi:10.2514/6.2014-1457, AIAA 2014-1457.

[3] Zhang, Q., and Liu, H. H. T., "Aerodynamics Modeling and Analysis of Close Formation Flight," *Journal of Aircraft*, Vol. 54, No. 6, 2017, pp. 2192–2204. doi:10.2514/1.C034271.

[4] Oh, K.-K., Park, M.-C., and Ahn, H.-S., "A survey of multi-agent formation control," *Automatica*, Vol. 53, 2015, pp. 424–440. doi:10.1016/j.automatica.2014.10.022.

[5] Yang, R., HaoZhang, Feng, G., Yan, H., and Wang, Z., "Robust cooperative output regulation of multi-agent systems via adaptive event-triggered control," *Automatical*, Vol. 102, 2019, pp. 129–136. doi:10.1016/j.automatica.2019.01.001.

[6] Dimarogonas, D. V., and Kyriakopoulos, K. J., "On the Rendezvous Problem for Multiple Nonholonomic Agents," *IEEE Transactions on Automatic Control*, Vol. 52, No. 5, 2007, pp. 916–922. doi:10.1109/TAC.2007.895897.

[7] Sun, Z., Anderson, B. D. O., Deghat, M., and Ahn, H.-S., "Rigid formation control of double-integrator systems," *International Journal of Control*, Vol. 90, No. 7, 2016, pp. 1403–1419. doi:10.1080/00207179.2016.1207100.

[8] Deghat, M., Anderson, B. D. O., and Lin, Z., "Combined Flocking and Distance-Based Shape Control of Multi-Agent Formations," *IEEE Transactions on Automatic Control*, Vol. 61, No. 7, 2016, pp. 1824–1837. doi:10.1109/TAC.2015.2480217.

[9] Lawton, J. R. T., Beard, R. W., and Young, B. J., "A Decentralized Approach to Formation Maneuvers," *IEEE Transactions on Robotics and Automation*, Vol. 19, No. 6, 2003, pp. 933–941. doi:10.1109/TRA.2003.819598.

[10] Ren, W., and Beard, R. W., "Decentralized Scheme for Spacecraft Formation Flying via the Virtual Structure Approach," *Journal of Guidance, Control, and Dynamics*, Vol. 27, No. 1, 2004, pp. 706–716. doi:10.2514/1.9287.

[11] Rezaee, H., and Abdollahi, F., "A Decentralized Cooperative Control Scheme With Obstacle Avoidance for a Team of Mobile Robots," *IEEE Transactions on Industrial Electronics*, Vol. 61, No. 1, 2014, pp. 347–354. doi:10.1109/TIE.2013.2245612.

[12] Dong, X., Zhou, Y., Ren, Z., and Zhong, Y., "Time-Varying Formation Tracking for Second-Order Multi-Agent Systems Subjected to Switching Topologies With Application to Quadrotor Formation Flying," *IEEE Transactions Industrial Electronics*, Vol. 64, No. 6, 2017, pp. 5014–5024. doi:10.1109/TIE.2016.2593656.

[13] Balch, T., and Arkin, R. C., "Behavior-based formation control for multirobot teams," *IEEE Transactions on Robotics and Automation*, Vol. 14, No. 6, 1998, pp. 926–939. doi:10.1109/70.736776.

[14] Pachter, M., Azzo, J. J. D., and Proud, A. W., "Tight Formation Flight Control," *Journal of Guidance, Control, and Dynamics*, Vol. 24, No. 2, 2001, pp. 246–254. doi:10.2514/2.4735.

[15] Dogan, A., and Venkataramanan, S., "Nonlinear Control for Reconfiguration of Unmanned-Aerial-Vehicle Formation," *Journal of Guidance, Control, and Dynamics*, Vol. 28, No. 4, 2005, pp. 667–678. doi:10.2514/1.8760.

[16] de Almeida, F. A., "Tight Formation Flight with Feasible Model Predictive Control," *Proceedings of AIAA Guidance, Navigation, and Control Conference*, AIAA, Kissimmee, Florida, U.S.A., 2015. AIAA 2015-0602.

[17] Gu, Y., Seanor, B., Campa, G., Rowe, M. R. N. L., Gururajan, S., and Wan, S., "Design and Flight Testing Evaluation of Formation Control Laws," *IEEE Transactions on Control Systems Technology*, Vol. 14, No. 6, 2006, pp. 1105–1112. doi:10.1109/TCST.2006.880203.

[18] Chichka, D. F., Speyer, J. L., Fanti, C., and Park, C. G., "Peak-Seeking Control for Drag Reduction in Formation Flight," *Journal of Guidance, Control, and Dynamics*, Vol. 29, No. 5, 2006, pp. 1221–1230. doi:10.2514/1.15424.

[19] Brodecki, M., and Subbarao, K., "Autonomous Formation Flight Control System Using In-Flight Sweet-Spot Estimation," *Journal of Guidance, Control, and Dynamics*, Vol. 38, No. 6, 2015, pp. 1083–1096. doi:10.2514/1.G000220.

[20] Zhang, Q., and Liu, H. H. T., "Aerodynamic model-based robust adaptive control for close formation flight," *Aerospace Science and Technology*, Vol. 79, 2018, pp. 5–16. doi:10.1016/j.ast.2018.05.029.

[21] Zhang, Q., and Liu, H. H. T., "UDE-Based Robust Command Filtered Backstepping Control for Close Formation Flight," *IEEE Transactions on Industrial Electronics*, Vol. 65, No. 11, 2018, pp. 8818–8827. doi:10.1109/TIE.2018.2811367.

[22] Diestel, R., *Graph Theory*, 2nd ed., Springer-Verlag, New York, NY, USA, 2000.

[23] Godsil, C., and Royle, G., *Algebraic Graph Theory*, Springer-Verlag, New York, NY, USA, 2000.

[24] Merris, R., "Laplacian matrices of graphs: a survey," *Linear Algebra and its Applications*, Vol. 197-198, 1994, pp. 143–176. doi:10.1016/0024-3795(94)90486-3.

[25] Zhong, Q.-C., and Rees, D., "Control of Uncertain LTI Systems Based on an Uncertainty and Disturbance Estimator," *Journal of Dynamic Systems, Measurement, and Control*, Vol. 126, No. 4, 2004, pp. 34–44. doi:10.1115/1.1850529.

[26] Zhu, B., Zhang, Q., and Liu, H. H.-T., "A Comparative Study of Robust Attitude Synchronization Controllers for Multiple 3-DOF Helicopters," *Proceedings of 2015 American Control Conference*, IEEE, Chicago, Illinois, 2015.

[27] Zhu, B., Zhang, Q., and Liu, H. H., "Design and experimental evaluation of robust motion synchronization control for multivehicle system without velocity measurements," *International Journal of Robust and Nonlinear Control*, Vol. 28, No. 17, 2018, pp. 5437–5463. doi:10.1002/rnc.4323.

[28] Khalil, H. K., *Nonlinear Systems*, 3rd ed., Prentice Hall, 2001.